EasyChair Preprint

№ 5964

Metal enhanced luminescence of Cerium Oxide (IV) Hollow Sub-microspheres with Au, AuPd and Pd Nanoparticles

Mario Guzmán, Dalia Chávez-García, Amanda Nieto, Karla Oyuky Juárez-Moreno and Andrey Simakov

June 30, 2021

Metal enhanced luminescence of Cerium Oxide (IV) Hollow Sub-microspheres with Au, AuPd and Pd Nanoparticles

Mario Guzmán, PhD.[1], Dalia Chávez-García, PhD.[1], Amanda Nieto, M.Sc. [1], Karla O. Juárez-Moreno[2,4], PhD and Andrey Simakov, PhD.[3]

[1] Centro de Enseñanza Técnica y Superior (CETYS), México, mario.guzman@cetys.mx, dalia.chavez@cetys.mx, amanda.nieto@cetys.mx.

[2] Departamento de Bionanotecnología, Universidad Nacional Autónoma de México, Centro de Nanociencias y Nanotecnología, México, kjuarez@cnyn.unam.mx.

[3] Departamento de Nanocatálisis, Universidad Nacional Autónoma de México, Centro de Nanociencias y Nanotecnología, México, andrey@cnyn.unam.mx.

[4] CONACYT-CNyN-UNAM, Ensenada, México

This work reports an analysis of the luminescent properties of Cerium oxide (IV) hollow sub-microspheres (CeO_2-HS) as well as the effect of the presence of Au, AuPd and Pd NPs over the mentioned properties. CeO_2-HS were synthesized via hydrothermal method, then the CeO_2-HS were impregnated with the metal precursors and by a reduction process the metal nanoparticles (NPs) were obtained. CeO_2-HS were characterized by XRD, Raman, UV-Vis and TEM. The CeO_2-HS with metal NPs deposited on them were analyzed using UV-Vis and TEM. All samples luminescent excitation and emission spectra were recorded. It was observed that the presence of metal NPs dramatically increases the emission intensity compared to the CeO_2-HS without metal NPs. Finally, it was also observed a clear slight but evident displacement of the main emission peak between samples with and without metal NPs

Keywords: Ceria, Hollow spheres, Metal enhanced luminescence, Noble metal NPs

I. INTRODUCTION

Cerium oxide (IV) (CeO_2) is a rare earth oxide that presents a considerable variety of applications. CeO_2 can be used as adsorbent material for pollutant compounds (1), support for heterogeneous catalysts (2), antimicrobial (3–5), cancer treatment (6), magnetic material (7,8) and as a luminescent material (9–11). The interest on the CeO_2 as a nanomaterial has recently increased due, not only to its remarkable properties, but also, to the variety of morphologies at the nanoscale such as cubes, rods, wires, particles and spheres (2,3,9,12); that can be obtained via relatively easy methods. Among these structures, hollow nanospheres (1,13,14) are a very promising material due to their possible application as nanoreactors (15), as drug delivery systems (16–18) and as drug carrier (19).

It has been previously reported that the luminescent intensity of the CeO_2 is related with the content of Ce^{3+} species which is also associated with the corresponding crystal sizes (20), but even when the CeO_2 presents photoluminescent properties, it does not present a high luminescence (9). Recently an interesting and useful strategy has been used for the enhancement of the luminescent properties of the lanthanides (21,22), which involves the addition of metal nanoparticles that presents a surface plasmon resonance which allows to increase the intensity of the photoemission. One of the most studied metal nanoparticle system is the gold nanoparticles (Au NPs). It is well known that the plasmonic resonance for the Au NPs depends on their shape and size as well as the nature of the media in which the Au NPs is dispersed. On the other hand, Palladium nanoparticles (Pd NPs) do not exhibit a plasmonic resonance in the visible spectrum. However, due to their similar atomic size and crystal structure it is possible to form bimetallic systems and, as a consequence, modify in a controlled manner the properties of such combination.

It is proposed that the interaction between the CeO_2 hollow spheres and the metal nanoparticles depends directly on the nature of these nanoparticles and that, the luminescence properties of these systems will be also affected by their metallic composition.

In the present work, we report the synthesis and characterization of cerium oxide (IV) hollow sub-microspheres with and without Au, AuPd and Pd nanoparticles, as well as an analysis of their luminescent properties and the enhancement effect of the metal nanoparticles over the ceria sub-microspheres luminescence.

II. MATERIALS AND METHODS

A. Synthesis of materials

Cerium chloride ($CeCl_3$*7 H_2O), urea (N_2H_4CO) and trisodium citrate anhydride ($Na_3C_6H_5O_7$) were purchased from Sigma Aldrich, hydrogen peroxide (H_2O_2 30%) was received from Fisher Chemical. Trichloroauric acid 99% ($HAuCl_4$) and Palladium Chloride (II) 99 % ($PdCl_2$) were purchased from Alfa-Aesar. All reagents were used without further purification.

Cerium oxide (IV) hollow sub-microspheres (CeO_2-HS) were prepared as reported by Qi et al. (23). In a typical synthesis 0.52 g of urea was dissolved in 85.5 ml of deionized water and stirred until obtain a clear solution. Then 36 ml of a 10 mM solution of $Na_3C_6H_5O_7$ was added to the previous solution, the mixture was stirred for 10 minutes. Subsequently, 0.89 g of $CeCl_3$*7H2O was added to the mixture under stirring for 15 minutes. Then 5 ml of H_2O_2 30 % was added dropwise during 30 minutes, turning the solution to a light-yellow color. The mixture was transferred to stainless steel autoclave. The system was heated to 100°C and maintained at this temperature for two hours; subsequently, the temperature was raised again up to 180°C and maintained for 18 h. The autoclave was cool down and a light-yellow powder was obtained. The powder was centrifuged and washed three times with deionized water, and finally dried at 80°C in air for 12 h.

Noble metal supported on the CeO_2-HS were synthesized as reported by (14) et al. In a typical synthesis, 0.2 g of the previous prepared CeO_2-HS was dispersed in 10 ml of deionized water. Then, 3.0 ml of a 10 mM solution of $HAuCl_4$ was added to the previous dispersion. The mixture was magnetically stirred for 12 hours and the centrifuged at 4000 rpm for 10 minutes. The precipitate was separated and re-dispersed in 10 ml of deionized water. At that point, 10 ml of a 0.1 M solution of $NaBH_4$ was added to the mixture and vigorously stirred for 15 minutes. Finally, the previous suspension (light purple color) was centrifuged at 4000 rpm for 10 minutes and washed with deionized water by triplicated. The solid obtained was dried at 80ºC for 12 hours, having a light purple powder as a final material (Au/CeO_2-HS). The procedure was repeated varying the metallic content (1.5 ml of $HAuCl_4$ 10 mM +1.5 ml of $PdCl_2$ 10 mM for the AuPd/CeO_2-HS sample, and 3.0 ml of $PdCl_2$ 10 mM for the Pd/CeO_2-HS sample).

B. Materials characterization:

Transmission electron microscopy (TEM) was used to analyze the structure of the CeO_2-HS with and without noble metal nanoparticles, using a JEOL JEM-2010 microscope with XMAX OXFORD detector. Previous for the analysis the samples were dispersed in propan-2-ol and dropped on a copper grid coated with carbon film. The crystallographic phases of CeO_2-HS were studied by X-Ray diffraction with a Philips X'pert MPD diffractometer, applying CuKa (0.154 nm) radiation. Crystallite size and crystalline strain were estimated from the Williamson-Hall (W-H) plot as reported by (24). W-H plot was obtained from the equation 1.

$$\beta_{hkl}\, cos\theta = \frac{K\lambda}{D} + 4\varepsilon\, sin\theta \qquad (1)$$

Where:

θ : The diffraction angle

β_{hkl}: The peak´s broadening

K: Shape's factor (equal to 0.9)

D: Crystallite size

Noble metal content (Au and Pd) in the samples was estimated by inductively coupled plasma-optical emission spectroscopy (ICP-OES), using a Vista pro (varian) equipment. Three different pattern solutions (1, 5 and 10 ppm) were used to calibrate the analysis.

Samples were prepared once as it follows. First, 20 mg of a sample was digested for 24 hours in an acid solution (1 ml of HNO_3 70% and 1 ml of HCl 30 %). Then, 1 ml of the previous solution was diluted in deionized water at a volume ratio of 1:25. Metal content was determined using the diluted solution.

The optoelectronic properties of all samples were studied UV-Vis spectroscopy in a diffuse reflectance mode. UV–visible spectra were collected using an Avaspec-2048 UV–visible spectrometer (Avantes) equipped with AvaLight-DHS light source and AvaSphere-30 integrating sphere. MgO was used as a reference. CeO_2-HS at different thermal treatments were studied by Raman System AvaSpec-ULS2048LTEC-USB2 (Avantes) equipped with two temperature-controlled diode lasers (power 500 mW, 785 nm excitation wavelength) were used. Luminescence analysis was performed using a Cary Eclipse Fluorescence Spectrometer, using an excitation wavelength of 510 nm and an emission wavelength of 254 nm, all samples were analyzed in aqueous media. The samples were dispersed in deionized water previous for the analysis (0.7 mg/ml).

III. RESULTS AND DISCUSSION:

The Cerium oxide (IV) hollow sub-microspheres (CeO_2-HS) were successfully obtained. Figure 1 (a) shows the TEM images for de CeO_2-HS (Fig. 1a), ceria spheres present a diameter around 250 nm. HR-TEM for all samples (Fig. 1e, f, g and h) shows an interplanar distance typical of the fluorite-type ceria (JCPDS No. 34-0394), corresponding to the (2 0 0) plane (d= 0.271 nm) and (2 0 0) plane (d= 0.192 nm). Metal nanoparticles have a quasi-spherical shape and sizes between 4.1 nm and 8.8 nm.

Digital Object Identifier: (only for full papers, inserted by LACCEI).
ISSN, ISBN: (to be inserted by LACCEI).
DO NOT REMOVE

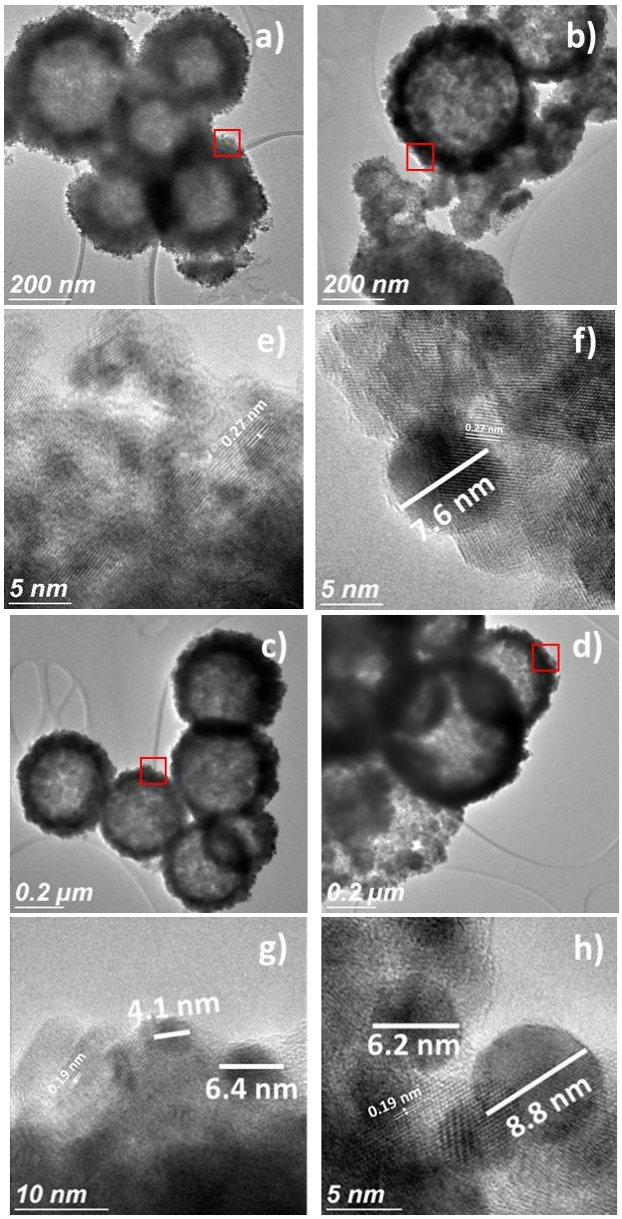

Figure 1 Typical TEM and HR-TEM images of CeO_2-HS (a and e), Au/ CeO_2-HS (b and f), AuPd/ CeO_2-HS (c and g) and Pd/ CeO_2-HS (d and h). High resolution TEM images correspond to the areas selected by red box.

The XRD pattern (Fig. 2 a) for the CeO_2-HS presents diffraction peaks at 28.62, 33.13, 47.61, 56.46, 59.33, 69.60, 76.90 and 79.06 values for the 2θ angle. The diffraction pattern corresponds to the ceria fluorite-type crystal structure (JCPDS 34-0394). The Fig. 2 (b) presents the W-H plot for the CeO_2-HS after thermal treatment at 500ºC for 6 hours. The crystallite size and the crystalline strain were estimated by the intercept and the slope of the W-H plot respectively. The crystal size for the CeO_2-HS sample was about 10.3 nm and the crystalline strain equal to $8.35*10^{-4}$.

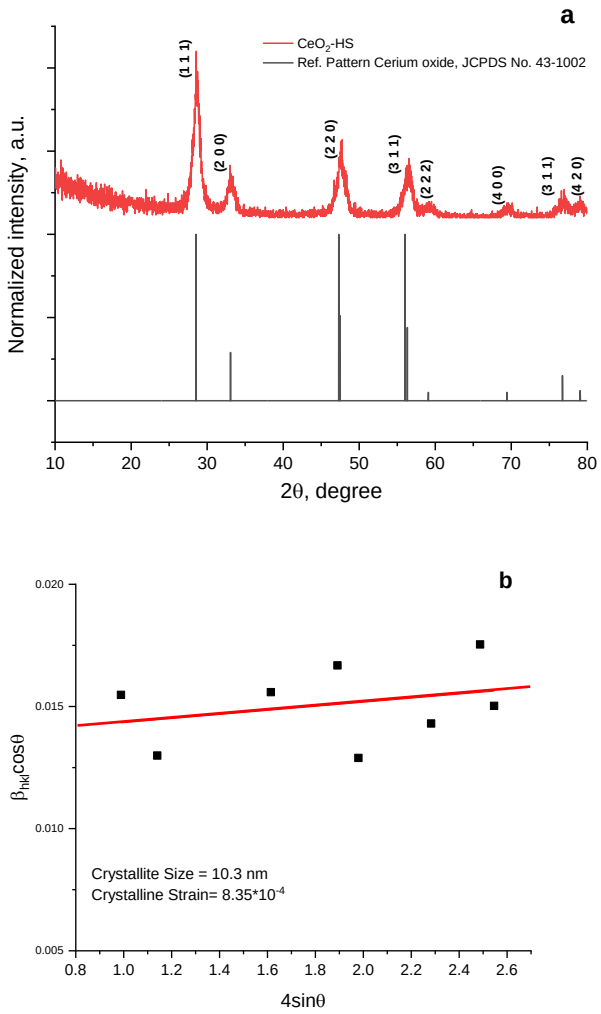

Figure 2.-XRD pattern (a) and W-H plot for CeO_2-HS (b).

Raman spectroscopy allows analyzing the structural defects content on the material. Fig. 3 shows two Raman spectra for CeO_2-HS before and after heat treatment. Both spectra, presents a characteristic peak centered around 464 cm^{-1} which corresponds to the symmetric mode F_{2g} for the CeO_2 (25). Raman spectroscopy for CeO_2-HS (Fig. 3) presents a typical F_{2g} peak centered at 464 cm^{-1} which is associated to the Ce-O bonding. The sample treated at 500º C has a remarkable higher intensity than the sample treated at 300º C, according to (26,27) the phase transition from $Ce(OH)_4$ to CeO_2 occurs about a temperature of 400º C which explains the increase in the intensity of the spectrum signal of the sample treated at 500º C. Also, there is a shoulder of the F_{2g} peak at 602 cm^{-1}. This shoulder is associated with oxygen vacancies in the material (3). The oxygen vacancies is commonly associated with the presence of Ce^{3+} species, that are usually linked to different properties such as compound adsorption (28), magnetic (29) and luminescent properties (9).

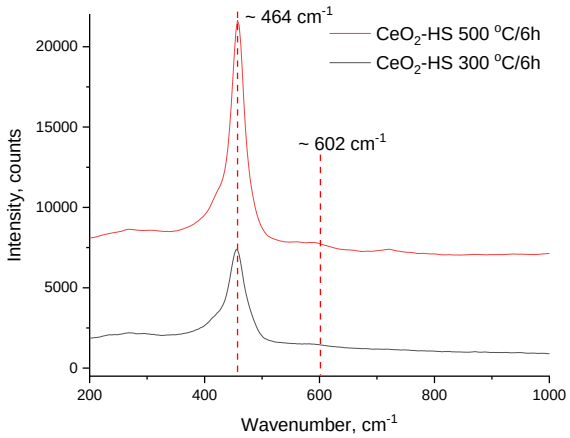

Figure 3.-Raman spectra of CeO_2-HS under different thermal treatments

Chemical composition of samples loaded with metal nanoparticles (Table 1) presents very similar metal content in each of the sample analyzed. Most of the metal employed during the synthesis remained present in the samples.

TABLE 1
. CHEMICAL QUANTIFICATION OF METAL CONTENT IN SAMPLES WITH METAL NANOPARTICLES

Sample	Ce, % weight	Au, % weight	Pd, (% weight)
Au@CeO_2	80.80	0.73	-
AuPd@CeO_2	80.54	0.53	0.52
Pd@CeO_2	80.57	-	1.02

The optoelectronic properties of the CeO_2-HS were studied by diffuse reflectance UV-Vis spectroscopy (DR-UV-Vis) (Fig. 4). The ceria spheres present a band gap around 3.1 eV which is similar to the value reported by (8), also Bazhukova (9) reported the same band gap with CeO_2 NPs suspension. The Ceria hollow spheres with Au NPs supported on it (Au/CeO_2-HS) presents a plasmonic resonance centered on 550 nm, which is an evidence of the presence of Au NPs in the material. It has been reported that AuNPs with diameter about the size of our system presents a plasmonic resonance around 521 nm (30,31). Nevertheless, the plasmon position depends on the dielectric function of the media which is in direct contact with the nanoparticles (32), which indicates that the difference between the plasmon position in the Au/CeO_2-HS and the position reported by (30,31) is associated with the electronic interaction between the cerium oxide (IV) and the Au NPs.

On the other hand, the spectrum for the bimetallic system (AuPd/CeO_2-HS) shows an evidently lower intensity on the gold's plasmon in comparison with the one observed for the Au/CeO_2-HS system. Chen et al. (33) reported that, for bimetallic AuPd NPs, the coating of Au NPs with Pd causes a gradual decrease over the intensity of the plasmonic resonance for the gold; based on this is possible to conclude that the AuPd/CeO_2-HS consists in bimetallic AuPd NPs instead of Au and Pd NPs. Finally, the Pd/CeO_2-HS system doesn't have any main features in the UV-Vis range that can be related to the presence of the Pd species, nevertheless there is a slightly change in the profile of the CeO_2 in comparison with the CeO_2-HS spectrum. Such difference might be associated with a modification of the semiconductor behavior of the CeO_2 due to the interaction with the Pd NPs.

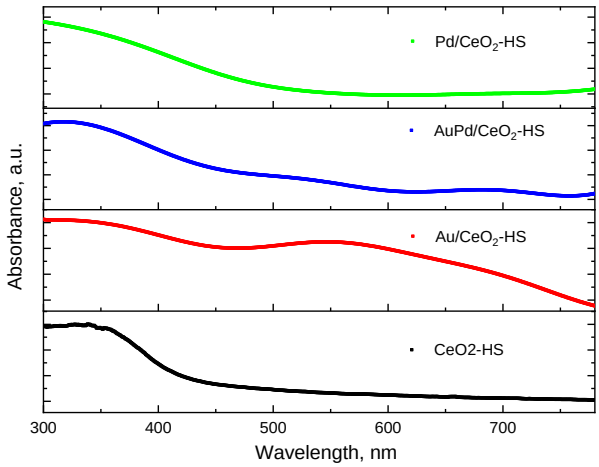

Figure 4. DR UV-Vis for CeO_2-HS (--), Au/CeO_2-HS (--), AuPd/ CeO_2-HS (--) and Pd/ CeO_2-HS (--).

To improve the photoluminescence (PL) intensity for CeO_2-HS NPs, we used the strategy of metal-enhanced luminescence (MEL) [21] this technique is based on the localized plasma effect of precious metal NPs, such as Au-NPs or Ag-NPs. This phenomenon happens when luminescence material is placed near metal NPs, in this case, the phosphors bring a mirror dipole in the metal NPs and it radiates the coupled quanta high efficiency that produce enhanced luminescence.

The PL spectra for CeO_2-HS NPs, Au/CeO_2-HS, AuPd/ CeO_2-HS and Pd/ CeO_2-HS is shown in figure 6, the excitation wavelength was 510 nm, the emission spectra of the CeO_2-HS NPs is 254 nm due to the electronic transition $^2F_{5/2}$ –> $5d_2$ with low intensity (figure 6A), as characteristic of nanoceria, with the addition of Au, Pd and Au/Pd the enhancement of the PL emission spectra is depicted. Au-NPs had the inherent ability to produce plasmonic resonance on the surface [34] and Pd tends to have more stability to bonds with surface oxygen atoms than surface metal atoms, this is correlated to the position of the d electron density center of Pd atom [35].

MEL phenomenon was explored by [21] with Ag@SiO_2 nanoparticles; they demonstrated that the luminescence intensity and quantum yield of the lanthanide complexes can be enormously enhanced by the Ag@SiO_2 with optimized size

under proper excitation wavelength. In figure 6B the enhanced luminescence is shown for nanoceria NPs and Au with excitation at 510 nm wavelengths, the emission is at 253-254 nm, the excitation spectra were measured and depicted in figure 7B at 508-510 nm.

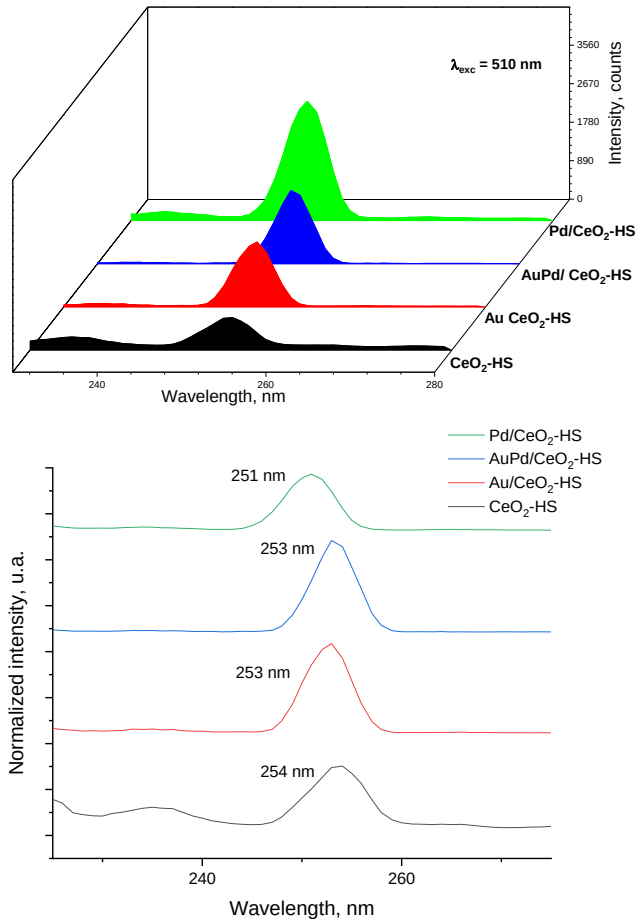

Figure 6.-PL spectra (Emission) for CeO_2-HS (**A**), Au/CeO_2-HS (**B**), AuPd/ CeO_2-HS (**C**) and Pd/ CeO_2-HS (**D**).

For Au-Pd/ CeO_2-HS and Pd/ CeO_2-HS NPs the emission spectra is shown in figures 6C and 6D, according to [34], they analyzed the binding energy for Au and Au/Pd core shell NPs and found a dependency of binding energies of Pd ($3d_{5/2}$) and Au ($4f_{7/2}$), with the increase of Pd content, the interaction between Au and Pd atoms gradually weakens and the dominant role of Pd atoms tend to determine the electronic structure. In figure 6D is observed that the enhanced luminescence is in the presence of Pd atoms into the nanoceria and in figure 6B it is observe that the combination of Au/Pd is similar to the Au-nanoceria NPs.

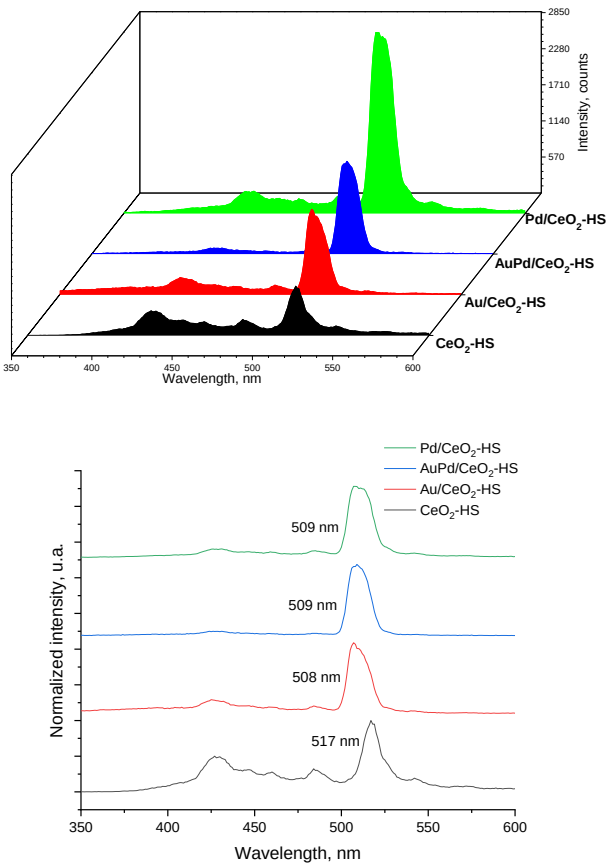

Figure 7.-PL spectra (Excitation) for CeO_2-HS (**A**), Au/CeO_2-HS (**B**), AuPd/ CeO_2-HS (**C**) and Pd/ CeO_2-HS (**D**).

IV. Conclusion:

The Cerium oxide (IV) hollow submicrospheres were successfully obtained via hydrothermal synthesis. CeO_2-HS photoluminescence presents an enhancement by the addition of Au, AuPd and Pd NPs on their surface. It was also observed that, the excitation peak centered around 517 nm presents a blue shift to the presence of the metal NPs. The observed blue shifts varied depending on the nature of the metal NPs (Au NPs > AuPd > Pd), same behavior was observed for the emission spectra, were the system containing Pd NPs presented a blue shift from 254 nm to 251 nm. The NPs, with the addition of Au, Pd and Au/Pd, observed enhancement of the PL emission spectra. Au-NPs produce plasmonic resonance that produces this enhancement. Finally based on the previously reported, we may conclude that Metal NPs-CeO_2 are promising materials for biomedical applications such as cancer detection via photoluminescence and photo-thermal cancer treatment.

ACKNOWLEDGMENT

The authors wish to acknowledge the support of CETYS University as well as to the Consejo Nacional de Ciencia y Tecnología (CONACYT) and to the proyect IN 206920 DGAPA PAPIIT.

REFERENCES

[1] Guzman M, Estrada M, Miridonov S, Simakov A. Synthesis of cerium oxide (IV) hollow nanospheres with tunable structure and their performance in the 4-nitrophenol adsorption. Microporous and Mesoporous Materials. 2019 Apr 1;278:241–50.

[2] Acosta B, Smolentseva E, Beloshapkin S, Rangel R, Estrada M, Fuentes S, et al. Gold supported on ceria nanoparticles and nanotubes. Applied Catalysis A: General. 2012;449:96–104.

[3] Krishnamoorthy K, Veerapandian M, Zhang L-H, Yun K, Kim SJ. Surface chemistry of cerium oxide nanocubes: Toxicity against pathogenic bacteria and their mechanistic study. Journal of Industrial and Engineering Chemistry. 2014 Sep 25;20(5):3513–7.

[4] Farias IAP, Santos CCL dos, Sampaio FC. Antimicrobial Activity of Cerium Oxide Nanoparticles on Opportunistic Microorganisms: A Systematic Review [Internet]. BioMed Research International. 2018 [cited 2021 Jan 12]. Available from: https://www.hindawi.com/journals/bmri/2018/1923606/

[5] Nadeem M, Khan R, Afridi K, Nadhman A, Ullah S, Faisal S, et al. Green Synthesis of Cerium Oxide Nanoparticles (CeO2 NPs) and Their Antimicrobial Applications: A Review. Int J Nanomedicine. 2020 Aug 11;15:5951–61.

[6] Diaconeasa A, Barbu-Tudoran L, Coman C, Leopold L, Mesaros A, Pop O, et al. Cerium Oxide Nanoparticles and Its Cytotoxicity Human Lung Cancer Cells. Romanian Biotechnological Letters. 2015;20(4):9.

[7] Niu X. Controlled hydrothermal synthesis of CeO2 nanospheres and their excellent magnetic properties. Appl Phys A. 2017 Mar 10;123(4):236.

[8] Phokha S, Pinitsoontorn S, Chirawatkul P, Poo-arporn Y, Maensiri S. Synthesis, characterization, and magnetic properties of monodisperse CeO2 nanospheres prepared by PVP-assisted hydrothermal method. Nanoscale Res Lett. 2012 Jul 31;7(1):425.

[9] Bazhukova IN, Sokovnin SYu, Ilves VG, Myshkina AV, Vazirov RA, Pizurova N, et al. Luminescence and optical properties of cerium oxide nanoparticles. Optical Materials. 2019 Jun 1;92:136–42.

[10] Gnanam S, Gajendiran J, Ramana Ramya J, Ramachandran K, Gokul Raj S. Glycine-assisted hydrothermal synthesis of pure and europium doped CeO2 nanoparticles and their structural, optical, photoluminescence, photocatalytic and antibacterial properties. Chemical Physics Letters. 2021 Jan 16;763:138217.

[11] Deus RC, Cortés JA, Ramirez MA, Ponce MA, Andres J, Rocha LSR, et al. Photoluminescence properties of cerium oxide nanoparticles as a function of lanthanum content. Materials Research Bulletin. 2015 Oct 1;70:416–23.

[12] Ketpang K, Oh K, Lim S-C, Shanmugam S. Nafion-porous cerium oxide nanotubes composite membrane for polymer electrolyte fuel cells operated under dry conditions. Journal of Power Sources. 2016;329:441–9.

[13] Deng W, Chen D, Chen L. Synthesis of monodisperse CeO2 hollow spheres with enhanced photocatalytic activity. Ceramics International. 2015 Nov;41(9):11570–5.

[14] Fan C-M, Zhang L-F, Wang S-S, Wang D-H, Lu L-Q, Xu A-W. Novel CeO2 yolk–shell structures loaded with tiny Au nanoparticles for superior catalytic reduction of p-nitrophenol. Nanoscale. 2012 Oct 11;4(21):6835–40.

[15] Evangelista V, Acosta B, Miridonov S, Smolentseva E, Fuentes S, Simakov A. Highly active Au-CeO2@ZrO2 yolk-shell nanoreactors for the reduction of 4-nitrophenol to 4-aminophenol. Applied Catalysis B: Environmental. 2015;166–167:518–28.

[16] Liu J, Qiao SZ, Chen JS, Lou XW (David), Xing X, Lu GQ (Max). Yolk/shell nanoparticles: new platforms for nanoreactors, drug delivery and lithium-ion batteries. Chem Commun. 2011 Nov 8;47(47):12578–91.

[17] Haag R. Supramolecular Drug-Delivery Systems Based on Polymeric Core–Shell Architectures. Angewandte Chemie International Edition. 2004;43(3):278–82.

[18] Huang C-C, Huang W, Yeh C-S. Shell-by-shell synthesis of multi-shelled mesoporous silica nanospheres for optical imaging and drug delivery. Biomaterials. 2011 Jan;32(2):556–64.

[19] Li JC, Jiang H, Wang XM. Preliminary application of cerium-based hollow nanospheres as drug carrier. IOP Conf Ser: Mater Sci Eng. 2018 Jun;380:012017.

[20] Génois R, Jobic S, Ouvrard G, Massuyeau F, Gautier R. The crucial impact of cerium reduction on photoluminescence. Applied Materials Today. 2020 Sep 1;20:100643.

[21] Zhao Y, Wang A, Kang J, Chu H, Zhang H, Zhao Y. Factors affecting the metal-enhanced luminescence of lanthanide complexes by Ag@SiO2 nanoparticles. Journal of Photochemistry and Photobiology A: Chemistry. 2020 Sep 1;400:112678.

[22] Ranjan R, Esimbekova EN, Kirillova MA, Kratasyuk VA. Metal-enhanced luminescence: Current trend and future perspectives- A review. Analytica Chimica Acta. 2017 Jun 8;971:1–13.

[23] Qi J, Zhao K, Li G, Gao Y, Zhao H, Yu R, et al. Multi-shelled CeO2 hollow microspheres as superior photocatalysts for water oxidation. Nanoscale. 2014;6(8):4072–7.

[24] Mote V, Purushotham Y, Dole B. Williamson-Hall analysis in estimation of lattice strain in nanometer-sized ZnO particles. J Theor Appl Phys. 2012 Jul 2;6(1):6.

[25] Li H, Zhang P, Li G, Lu J, Wu Q, Gu Y. Stress measurement for nonstoichiometric ceria films based on Raman spectroscopy. Journal of Alloys and Compounds. 2016 Oct 15;682:132–7.

[26] Vratny F, Kern S, Gugliotta F. The thermal decomposition of cerium (III) nitrate hydrate. Journal of Inorganic and Nuclear Chemistry. 1961 Jun 1;17(3):281–5.

[27] Guo Z, Du F, Li G, Cui Z. Synthesis and Characterization of Single-Crystal Ce(OH)CO3 and CeO2 Triangular Microplates. Inorg Chem. 2006 May 1;45(10):4167–9.

[28] Seo J, Moon J, Kim JH, Lee K, Hwang J, Yoon H, et al. Role of the oxidation state of cerium on the ceria surfaces for silicate adsorption. Applied Surface Science. 2016 Dec 15;389:311–5.

[29] Dutta P, Pal S, Seehra MS, Shi Y, Eyring EM, Ernst RD. Concentration of Ce3+ and Oxygen Vacancies in Cerium Oxide Nanoparticles. Chem Mater. 2006 Oct 1;18(21):5144–6.

[30] Liz-Marzán LM, Giersig M, Mulvaney P. Synthesis of Nanosized Gold−Silica Core−Shell Particles. Langmuir. 1996 Jan 1;12(18):4329–35.

[31] Link S, El-Sayed MA. Size and Temperature Dependence of the Plasmon Absorption of Colloidal Gold Nanoparticles. J Phys Chem B. 1999 May 1;103(21):4212–7.

[32] Miller MM, Lazarides AA. Sensitivity of Metal Nanoparticle Surface Plasmon Resonance to the Dielectric Environment. J Phys Chem B. 2005 Nov 1;109(46):21556–65.

[33] Chen X, Pan H, Liu H, Du M. Nonenzymatic glucose sensor based on flower-shaped Au@Pd core–shell nanoparticles–ionic liquids composite film modified glassy carbon electrodes. Electrochimica Acta. 2010 Dec 30;56(2):636–43.

[34] Li X, Li C, Xiang D, Zhang C, Xia L, Liu X, et al. Self-limiting synthesis of Au–Pd core–shell nanocrystals with a near surface alloy and monolayer Pd shell structure and their superior catalytic activity on the conversion of hexavalent chromium. Applied Catalysis B: Environmental. 2019 Sep 15;253:263–70.

[35] Ohkawa K, Noguchi Y, Nakayama S, Hashimoto K, Fujishima A. Electrochemical reduction of carbon dioxide on hydrogen-storing materials: Part 3. The effect of the absorption of hydrogen on the palladium electrodes modified with copper. Journal of Electroanalytical Chemistry. 1994 Mar 4;367(1):165–73.